CFD Investigation of Hydrodynamic Force and Moment Acting on Stern-Rudder Plane Configurations of a Submarine

Tien Thua Nguyen *, Thanh Long Phan, Thi Loan Mai

Posted Date: 7 April 2024

doi: 10.20944/preprints202404.0444.v1

Keywords: submarine; stern rudder -plane configuration; rudder force and moment; RANS-based simulation

Article

CFD Investigation of Hydrodynamic Force and Moment Acting on Stern-Rudder Plane Configurations of a Submarine

Tien Thua Nguyen [1,*], Thi Loan Mai [2] and Thanh Long Phan [1]

[1] The University of Danang – University of Science and Technology; ntthua@dut.udn.vn, ptlong@dut.udn.vn
[2] Changwon National University; mailoankttt@gmail.com
* Correspondence: ntthua@dut.udn.vn

Abstract: The paper presents the prediction of hydrodynamic characteristics of different rudder plane configurations behind a submarine in deep water through Reynolds-Averaged Navier-Stokes method in Ansys Fluent Solver. The hydrodynamic force and moment acting on the Cross-plane, X-plane, and Y-plane rudder configurations are analyzed for estimating hydrodynamic coefficients. The obtained results show that X-force of the X-plane rudder configuration is larger than the force acting on the Cross-plane rudder and Y-plane rudder configurations. However, Y-force, and Z-force of the X-plane rudder configuration are significantly greater than the Y-force of the left configurations. The same tendency can be seen in the moment of the X-plane rudder about the y-axis and z-axis. The roll moment induced by the Y-plane and Cross-plane rudder configurations is significantly larger than the case of the X-plane rudder configuration.

Keywords: submarine; stern rudder plane configuration; rudder force and moment; RANS-based simulation

1. Introduction

The maneuvering characteristics is one of the most important performances of the marine vehicles such as submarine. The rudder-plane configurations have a significant effect to control the ship journey. Hence, the hydrodynamic force and moment of different rudder-plane configurations are needed to analyze. Three types of rudder-plane configurations such as Cross-plane, X-plane, and Y-plane rudders are often equipped on the submarine. Each type of the rudder-plane configuration had been applied to predict the maneuvering characteristics of the submerged body as shown in [1–4].

The CFD (Computational Fluid Dynamics) method is widely used in the prediction of hydrodynamics acting on the marine vehicle due to its advantages. Nguyen [1] simulated virtual captive model test in Ansys Fluent for a full-scale submarine with a Cross-plane rudder configuration for estimating hydrodynamic coefficients. The virtual captive model tests of BB2 submarine in CFD-based simulation were performed by Cho et. al. [2] for the prediction of hydrodynamic forces and moment acting on the hull and the X-rudder plane configuration. Hydrodynamic forces, moments, and added masses of the submarine hull were obtained for evaluating the maneuvering characteristics of the submarine with six degrees of freedom. The thrust and moment of the propeller were estimated in open water condition. The turning ability of the submarine was verified with the results obtained from free-running model tests. The free running test of an underwater vehicle with six-degrees of freedom based on CFD method was implemented by Kim et. al [5]. Straight line and steady turning maneuver of the vehicle were also performed. The results showed that maneuvering characteristics of the vehicle were in good with the experimental results. An Autonomous Underwater Vehicle (AUV) with X-rudder plane configuration was also presented by Zhang et. al. [6]. The hydrodynamic force and moment of the X-rudder plane were predicted and compared with

 doi:10.20944/preprints202404.0444.v1

the results of Cross-rudder plane configuration. An X-rudder configuration for the autonomous underwater vehicle was tested by Zang et. al. [7] and the hydrodynamic characteristics of the body and rudders were then introduced to the equation of motion and control of the vehicle. Maneuvering behaviors of the model of CRN-INSEAN 2475 submarine with X-rudder or C-rudder configurations were predicted by Broglia et. al. [8]. The trajectory parameters of turning motion of the submarine were predicted for the angle of attacks of 5, 10, and 15 degrees. It is proved that the turning characteristics of the flapped X-rudder configuration are better than the turning behavior of the submarine using conventional X-plane rudder configurations. The captive model tests of the DARPA, SWE, and SMG submarines were carried out by Piaggio et. al. [9] for predicting hull forces and rudder forces for prediction of the maneuvering characteristics. The failure of the stern steering of the submarine with X-rudder plane or Cross-rudder plane configurations was also investigated. Hydrodynamic force and moment of an underwater vehicle with Cross-rudder plane configuration were obtained through CFD-based simulation of rotating arm test, drift test, rudder test and the combination tests between rotating arm and rudder deflection or drift-rudder, [10]. The obtained hydrodynamic coefficients were then introduced into the equations of the turning motion for evaluating the turning behavior of the vehicle. The latering force and yaw moment of the Cross-skeg rudder and X-rudder configurations were predicted through experimental method by Ke et. al., [11]. The axial velocites of fluid flow induced by the rudder plane configurations were investigated. The stern of SUBOFF-G submarine with a propeller and the Cross-skeg rudder configuration was automatic maneuverd for carrying out of the forward running and diving motion. The propeller thrust and resistance of the submarine obtainded from the virtual self-propulsion test were compared for finding the rotational speed of the propeller, [12]. Also, the visual of unsteady fluid flow surround the submarine with the propller and Cross-rudder plane configuration was investigated. The turing ability of a submarine with the X-rudder plane configuration and virtual propeller was predicted by numerical simulation of turning circles with different deflection of the rudders in Star-CMM+ code as shown in [13]. The complex fluid flow around the DARPA SUBOFF submarine with rudder deflection was analyzed based on OpenFOAM [14]. Hydrodynamic force and moment of the rudder with a wide range of deflection angles were calculated and compared with the experimental data. The forward running of a submarine near free water surface were simulated by Ansys Fluent code for predicting the resistance of the hull with Cross-rudder plane configuration and the thrust and torque of the propeller, [15]. The obtained results showed that the resistance of the hull and rudder plane near free surface are increased by 129-174% in comparision with the resistance of the submarine in deep water condition. The straight ahead motion and side-slip motion of 10 degrees of the model of DSTO generic submarine with full apendages were investigated by RANS (Reynolds-averaged Navier-stokes) and LES (Large Eddy Simulation) methods [16]. The fluid flow characteristics obtained from the numerical simulation such as axial velocity profiles, displacement of vortex core and turbulent intensity, were compared with the experimental results.

In this study, three types of rudder configuration located in the stern of a submarine will be analyzed using Ansys Fluent code. Hydrodynamic forces and moments acting on the X-plan rudder, Y-plane, and Cross-plane rudder configurations are numerically predicted. The best stern-plane rudder configuration from the point of view of the submarine's maneuvering characteristics will be analyzed.

2. Methodology

2.1. Coordinate Systems and Symbols

For predicting behaviors of the submarine, body-fixed ($Oxyz$) and earth-fixed ($O_1x_0y_0z_0$) coordinate systems are used for presenting dynamic behavior of the vehicle and its trajectory. The origin of the body-fixed coordinate system is located at the center of the mid section of the submarine. Figure 1 illustrates the two coordinate systems and definition of kinematics, forces, and moments of the submarine in which u, v, and w stand for linear velocities along the x, y, and z-axes and p, q, and r are angular velocities about the axes. X, Y, and Z indicate hydrodynamic forces of the control plane

Preprints.org (www.preprints.org) | NOT PEER-REVIEWED | Posted: 7 April 2024 doi:10.20944/preprints202404.0444.v1

along the x, y, and z-axes and K, M, and N are the moments of the control surface about x, y, and z-axes, correspondingly.

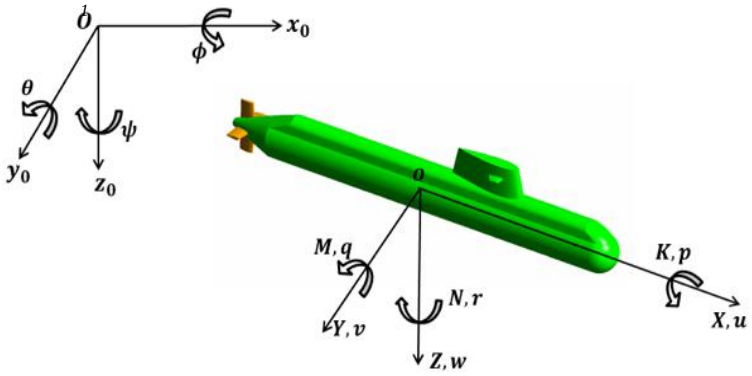

Figure 1. Coordinate systems and symbols.

2.2. Equation of Motion of the Submarine

Considering the submarine motion with six degrees of freedom, the equations of submarine's motion in calm water in the body-fixed coordinate system are described by Fossen [17], as shown in the following equations.

$$m[\dot{u} - vr + wq - x_G(q^2 + r^2) + y_G(pq - \dot{r}) + z_G(pr + \dot{q})] = X \tag{1}$$

$$m[\dot{v} - wp + ur - y_G(r^2 + p^2) + z_G(qr - \dot{p}) + x_G(qp + \dot{r})] = Y \tag{2}$$

$$m[\dot{w} - uq + vp - z_G(p^2 + q^2) + x_G(rp - \dot{q}) + y_G(rq - \dot{p})] = Z \tag{3}$$

$$\begin{aligned} I_x\dot{p} + (I_z - I_y)qr - I_{xz}(\dot{r} + pq) + I_{yz}(r^2 - q^2) + I_{xy}(qp - \dot{q}) \\ +m[y_G(\dot{w} - uq + vp) - z_G(\dot{v} - wp + ur)] = K \end{aligned} \tag{4}$$

$$\begin{aligned} I_y\dot{q} + (I_x - I_z)rp - I_{xy}(\dot{p} + qr) + I_{zx}(q^2 - p^2) + I_{yz}(qp - \dot{r}) \\ +m[z_G(\dot{u} - vr + wq) - x_G(\dot{w} - uq + vp)] = M \end{aligned} \tag{5}$$

$$\begin{aligned} I_z\dot{r} + (I_y - I_x)pq - I_{yz}(\dot{q} + rp) + I_{xy}(q^2 - p^2) + I_{zx}(rq - \dot{p}) \\ +m[x_G(\dot{v} - wp + ur) - y_G(\dot{u} - vr + wq)] = N \end{aligned} \tag{6}$$

Regarding the submarine motion in calm water, the external force and moment in the right side of the equations can be divided into hull forces (F_H) propeller forces (F_P) and control forces (F_C). For steering the submarine with six degrees of freedom, the control force and moment of the rudders and stabilizers should be determined. Hydrodynamic coefficients of the control plane are then analyzed using the Taylor expansion as shown in following equations.

$$F(X, Y, Z, K, M, N) = F_H + F_P + F_C \tag{7}$$

$$X_C = X_{\delta_r\delta_r}\delta_r^2 + X_{\delta_s\delta_s}\delta_s^2 \tag{8}$$

$$Y_C = Y_{\delta_r}\delta_r + Y_{\delta_r|\delta_r|}\delta_r\ |\delta_r| \tag{9}$$

$$Z_C = Y_{\delta_s}\delta_s + Y_{\delta_s|\delta_s|}\delta_s\ |\delta_s| \tag{10}$$

$$K_C = K_{\delta_r}\delta_r + K_{\delta_r|\delta_r|}\delta_r\ |\delta_r| \tag{11}$$

$$M_C = M_{\delta_s}\delta_s + M_{\delta_s|\delta_s|}\delta_s\ |\delta_s| \tag{12}$$

 doi:10.20944/preprints202404.0444.v1

$$N_C = N_{\delta_r}\delta_r + N_{\delta_r|\delta_r|}\delta_r\ |\delta_r| \tag{13}$$

2.2. Simulation Method

The Reynolds-Averaged Navier-Stokes (RANS) method is opted for analyzing the fluid flow over the submarine. Following the method, the instantaneous velocity is decomposed into its time-averaged and fluctuating velocity in which fluctuating velocity is modeled as a function of turbulence eddy viscosity and turbulence kinetic energy. The governing equations of the RANS method for incompressible flow are introduced by Menter [18] and Wilcox [19] as follows.

$$\frac{\partial \overline{u}_i}{\partial x_i} = 0 \tag{14}$$

$$\frac{\partial \overline{u}_i}{\partial t} + \overline{u}_j\frac{\partial \overline{u}_i}{\partial x_j} = -\frac{\partial \overline{p}}{\partial x_i} + \nu\frac{\partial^2 \overline{u}_i}{\partial x_j \partial x_j} - \frac{\partial \tau_{ij}}{\partial x_j} \tag{15}$$

The Reynolds stress, $\tau_{ij} = \overline{u_i' u_j'}$, is modeled as the function of eddy viscosity and kinetic energy based on the Boussinesq hypothesis. The turbulent model, *k-ω* SST (Shear Stress Transport), for solving turbulent flow around the submarine is presented as following, [18]:

$$\frac{\partial k}{\partial t} + \bar{u}_i\frac{\partial k}{\partial x_i} = P_k - \beta^*\omega k + \frac{\partial}{\partial x_j}\left((v + \sigma_k v_t)\frac{\partial k}{\partial x_i}\right) \tag{16}$$

$$\frac{\partial \omega}{\partial t} + \bar{u}_i\frac{\partial \omega}{\partial x_i} = \frac{\gamma}{\mu_t}P_k - \beta\omega^2 + \frac{\partial}{\partial x_j}\left[(v + \sigma_\omega v_t)\frac{\partial \omega}{\partial x_i}\right] + 2(1 - F_1)\frac{\sigma_{\omega 2}}{\omega}\frac{\partial k}{\partial x_i}\frac{\partial \omega}{\partial x_i} \tag{17}$$

$$\mu_t = \frac{\rho a_1 k}{max(a_1\omega, \Omega F_2)} \tag{18}$$

where P_k is the production rate of turbulent kinetic energy by the mean flow. The variables are defined as follows.

$$P_k = \tau_{ij}\frac{\partial u_i}{\partial x_j}$$

$$\tau_{ij} = \mu_t\left(2S_{ij} - \frac{2}{3}\frac{\partial u_k}{\partial x_k}\delta_{ij}\right) - \frac{2}{3}\rho k\delta_{ij}$$

$$S_{ij} = \frac{1}{2}\left(\frac{\partial u_i}{\partial x_j} + \frac{\partial u_j}{\partial x_i}\right)$$

$$\beta_i = F_1\beta_{i,1} + (1 - F_1)\beta_{i,2}$$

$$\sigma_k = \frac{1}{F_1/\sigma_{k,1} + (1 - F_1)\sigma_{k,2}}$$

$$\sigma_\omega = \frac{1}{F_1/\sigma_{\omega,1} + (1 - F_1)\sigma_{\omega,2}}$$

$$F_1 = \tanh(\arg_1^4)$$

$$F_2 = \tanh(\arg_2^2)$$

$$arg_1 = min\left[max\left(\frac{\sqrt{k}}{\beta^*\omega y}; \frac{500\nu}{y^2\omega}\right), \frac{4\rho\sigma_{\omega_2}k}{CD_{k\omega}y^2}\right]$$

Preprints.org (www.preprints.org) | NOT PEER-REVIEWED | Posted: 7 April 2024 doi:10.20944/preprints202404.0444.v1

$$arg_2 = max\left(2\frac{\sqrt{k}}{0.09\omega y};\frac{500\nu}{y^2\omega}\right)$$

$$CD_{k\omega} = max\left(2\rho\sigma_{\omega,2}\frac{1}{\omega}\frac{\partial k}{\partial x_i}\frac{\partial \omega}{\partial x_i}, 10^{-20}\right)$$

with the model constants are: $\sigma_{k,1}$=1.176, $\sigma_{\omega,1}$=2.0, $\sigma_{k,2}$=1.0, $\sigma_{\omega,2}$=1.168, a_1=0.31, $\beta_{i,1}$=0.075, $\beta_{i,2}$=0.0828.

3. Numerical Modelling

3.1. Case Study

The full-scale submarine is chosen as a target body in this study. Three stern-rudder plane configurations such as Cross-plane rudders, X-plane rudders, and Y-plane rudders with the same span of 7.4m are considered. The stern-rudder plane configurations are created from NACA0020 profile. Figure 2 presents the geometry and main dimensions of the rudder plane configurations and the submarine. Also, the definition of hydrodynamic force and moment acting on the Cross-rudder plane, X-rudder plane and Y-rudder plane configurations is shown in Figure 3. The two opposite blades in X-rudder plane and Cross-rudder plane configurations are all deflected about the same rotational axis that are parallel and 0.578 meters from the leading eadge. Meanwhile, a couple of blades in the Y-rudder plane configuration are rotated about the rotational axes with the same distance from the leading eadge but different direction. The rudder deflection, δ_r, is defined for each type of the rudder plane configuration as shown in Eq. 19~21. Also, the angle of deflection of each stabilizer, δ_s, is described in the left equations.

$$\delta_{r\_Cross} = \frac{(\delta_2 + \delta_4)}{2} \tag{19}$$

$$\delta_{r\_X} = \frac{(\delta_1 + \delta_2 + \delta_3 + \delta_4)}{4} \tag{20}$$

$$\delta_{r\_Y} = \frac{\delta_1 + \delta_2 + \delta_3}{3} \tag{21}$$

$$\delta_{s\_Cross} = \frac{(-\delta_1 - \delta_3)}{2} \tag{22}$$

$$\delta_{s\_X} = \frac{(-\delta_1 + \delta_2 - \delta_3 + \delta_4)}{4} \tag{23}$$

$$\delta_{s\_Y} = \frac{(\delta_2 - \delta_3)}{2} \tag{24}$$

Preprints.org (www.preprints.org) | NOT PEER-REVIEWED | Posted: 7 April 2024 doi:10.20944/preprints202404.0444.v1

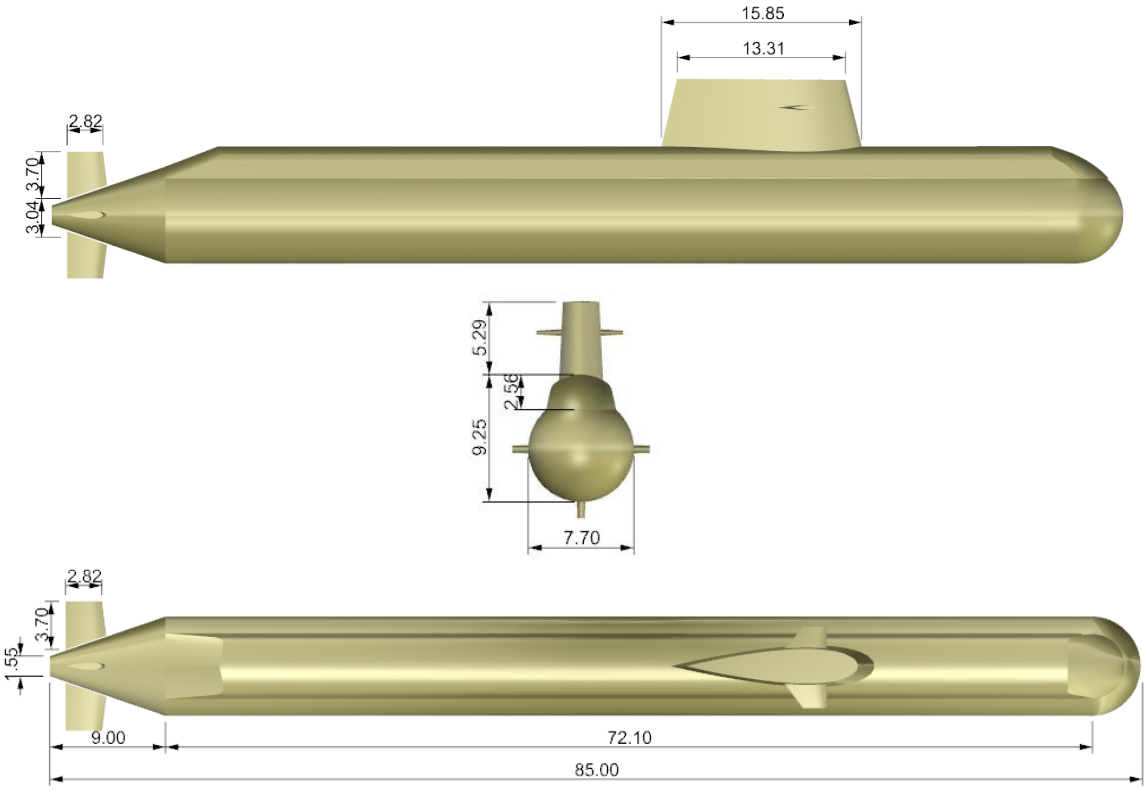

Figure 2. Main dimensions of the stern rudder configurations.

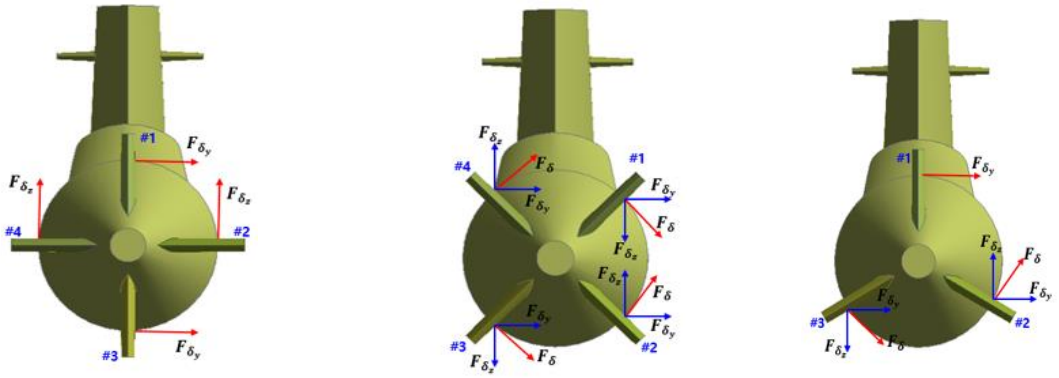

(**a**) Cross-plane (**b**) X-plane (c) Y-plane

Figure 3. Definition of the Cross-rudder plane, X-rudder plane and Y-rudder plane configurations and their hydrodynamic force and moment.

$$\delta_{r\_Cross} = \frac{(\delta_2 + \delta_4)}{2} \tag{19}$$

$$\delta_{r\_X} = \frac{(\delta_1 + \delta_2 + \delta_3 + \delta_4)}{4} \tag{20}$$

$$\delta_{r\_Y} = \frac{\delta_1 + \delta_2 + \delta_3}{3} \tag{21}$$

$$\delta_{s\_Cross} = \frac{(-\delta_1 - \delta_3)}{2} \tag{22}$$

Preprints.org (www.preprints.org) | NOT PEER-REVIEWED | Posted: 7 April 2024 doi:10.20944/preprints202404.0444.v1

$$\delta_{s\_X} = \frac{(-\delta_1 + \delta_2 - \delta_3 + \delta_4)}{4} \quad (23)$$

$$\delta_{s\_Y} = \frac{(\delta_2 - \delta_3)}{2} \quad (24)$$

3.2. CFD-Based Modeling

A rectangular shape will be selected as a fluid domain for simulating fluid flow over the submarine without the effect of reverse flow. Following ITTC Recommendation [20], the rectangular domain with 6L in length, 4L in breadth and 3L in height is created. The distance from the bow of the submarine to the front surface of the fluid domain is set as 2L, where L stands for the whole length of the submarine. The submarine is located at the middle of the fluid domain. In addition, physical conditions should be applied to the outer surfaces of the fluid domain. The submarine speed is assigned for the front surface as velocity inlet and pressure-outlet condition is applied for the back surface. Symmetry condition is set for the side, top, and bottom surfaces. No-slip wall condition is set on the surfaces of the submarine hull and control surfaces. Figure 4 presents the fluid domain and the boundary conditions on the submarine and outer surfaces.

To prepare for the simulation, the fluid domain is discrete using tetrahedral elements as shown in Figure 5. The boundary layer of fluid flow surrounding the submarine is modeled by layers of prism elements. The first layer thickness is determined from the dimensionless wall distance – y plus value. With the submarine speed of 20 knots, the Reynolds number is 1.0E+09 and the regime of fluid flow over the submarine and control surfaces is fully turbulence. According to Oh et. al. [21], the value of y plus is given about 3000~5000 for Re = 1.0E+09. Therefore, the value of y plus is chosen as 3000 and the height of the first layer thicknesses on the hull and the stern rudder plane configuration is then calculated as 9.0 millimeters.

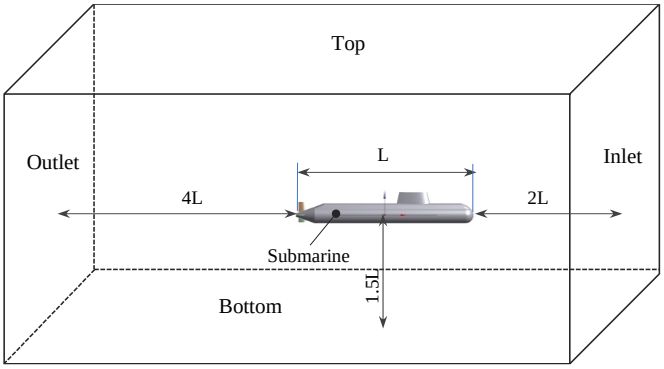

Figure 4. Fluid domain and boundary conditions.

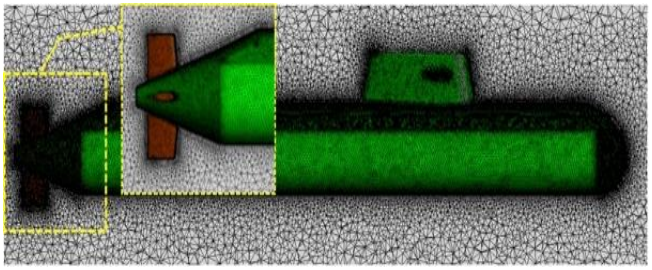

Figure 5. Local mesh in stern area and lobal mesh around the submarine.

The incompressible RANS solver in Ansys Fluent is used to simulate fluid flow through the submarine with the three rudder plane configurations. According to ITTC recommendation [20], the two-equation models of turbulence model, turbulent model of *k-ε* realizable or turbulence model of

Preprints.org (www.preprints.org) | NOT PEER-REVIEWED | Posted: 7 April 2024 doi:10.20944/preprints202404.0444.v1

k- ω SST (Shear Stress Transport) are recommended to use for simulating turbulent flow around the submarine motion. Thus, *k-ω* SST turbulence model is selected for modeling turbulent fluid flow through the submarine. The pressure field is obtained by solving the momentum equation using SIMPLE (Semi-Implicit Pressure Link Equation) algorithm. The second order upwind method is employed for estimating the face values from interpolation of cell center values and interpolation of pressure values.

4. Results

To verify the simulation results, the force along y-axis and moment about z-axis of the X-rudder plane configuration obtaind from the CFD-based simulation in Ansys Fluent are compared with the corresponding force and moment of a similar model (SWE submarine) that estimated by Piaggio et. al [9], as shown in Figure 6. It can be seen that the current results are complied with the experimental results and numerical simulation will be applied for estimation of hydrodynamic force and moment of the rudder plane configurations.

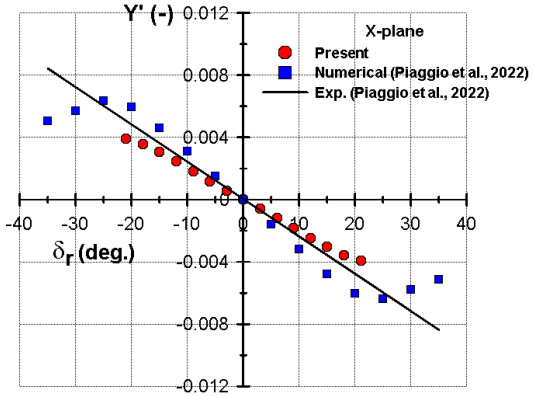

(**a**) Y-force of rudders versus angle of attack of the rudder

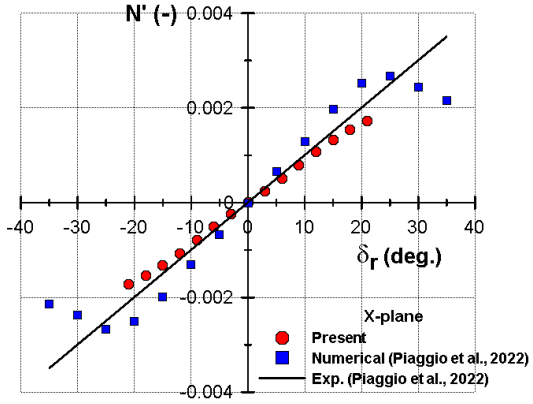

(b) Y-force of rudders versus angle of attack of the rudders

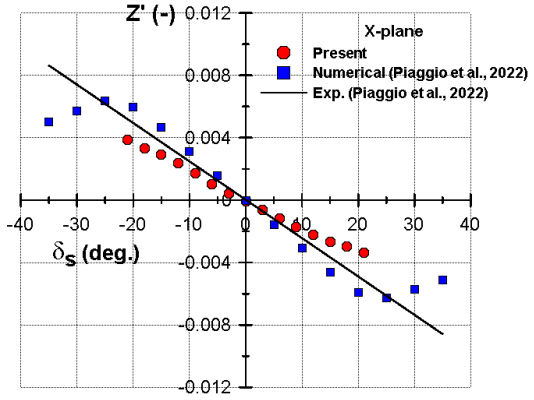

(c) Y-force of rudders versus angle of attack of the stabilizers

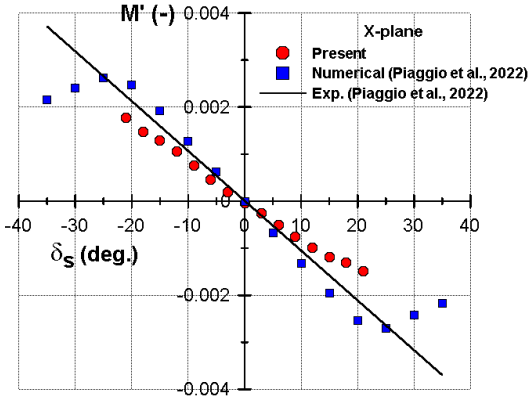

(d) Y-force of rudders versus angle of attack of the stabilizers

Figure 6. Comparison between currents results and the previous results of rudders and stabilizers on the SWE submarine in [9].

For predicting the hydrodynamic force and moment acting on the rudders and stabilizers, the submarine is forced to run steadily at the speed of 20 knots for different angles of the rudder and stabilizer. Both the rudder and stabilizer are rotated from 0 to 21 degrees about z-axis and y-axis, respectively. The interval of deflected angle for the simulation is 3 degrees for the cases. Because the submarine is a symmetrical body, the rudders will be rotated in one direction and the obtained results will be presented in both rotating directions. However, it is necessary to rotate the stabilizers in both

Preprints.org (www.preprints.org) | NOT PEER-REVIEWED | Posted: 7 April 2024 doi:10.20944/preprints202404.0444.v1

directions about its rotation axes. The hydrodynamic force and moment acting on each rudder-plane are estimated through the numerical simulation. Figure 7 presents the results of hydrodynamic force and moment acting on the X-rudder plane, Y-rudder plane, and Cross-rudder plane configurations that obtained from the CFD-based simulation. It can be seen that the hydrodynamic force and moment are increased as deflection angle of the rudder and stabilizer increases. The hydrodynamic forces along the *x* and *y*-axes of X-rudder plane are larger than the corresponding forces acting on the Cross-rudder plane and Y-rudder plane. The roll moment of the X-rudder plane is rather small in comparison with the moment acting on the left rudder plane configurations. This can be explained by the symmetry arrangement of the X-rudder configuration that induces the small value in hydrodynamic force along the z-axis and roll moment as well. In addition, the hydrodynamic force and moment acting on the Cross-rudder plane are slightly smaller than the force and moment of the Y-rudder plane. The similar trend can be found in hydrodynamic forces and moment acting on the stabilizers, as shown in Figure 8. The X-force, Y-force, and moment about y-axis of the stabilizers in X-rudder plane configuration is significantly larger than the X-force of stabilizers in the Cross-rudder plane and Y-rudder plane configurations.

The variation of hydrodynamic force and moment of the stern rudder plane configurations are then fitted using the least square method for estimating the hydrodynamic coefficients of the rudders and stabilizers. Table 1 depicts the hydrodynamic coefficient of the stern-rudder plane configurations.

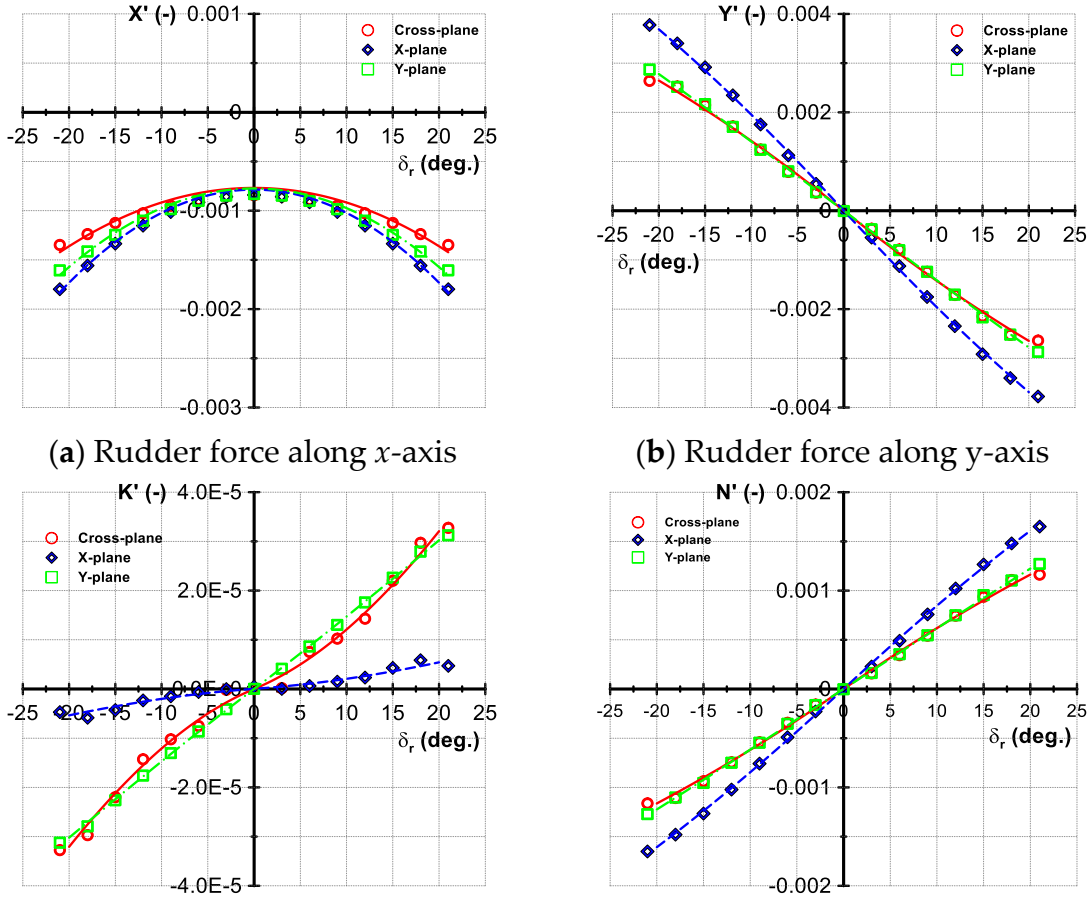

(**a**) Rudder force along *x*-axis (**b**) Rudder force along y-axis

(**c**) Rudder moment about *x*-axis (**d**) Rudder moment about z-axis

Figure 7. Hydrodynamic force and moment of the rudders in horizontal plane.

Preprints.org (www.preprints.org) | NOT PEER-REVIEWED | Posted: 7 April 2024 doi:10.20944/preprints202404.0444.v1

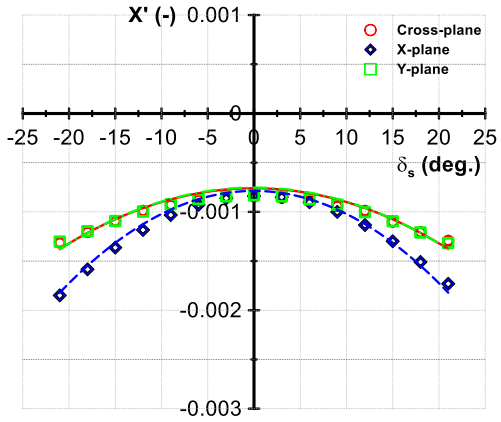

(**a**) X-force of the stabilizers

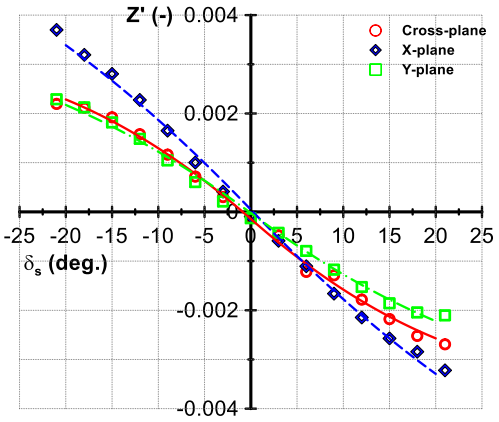

(**b**) Y-force of the stabilizers

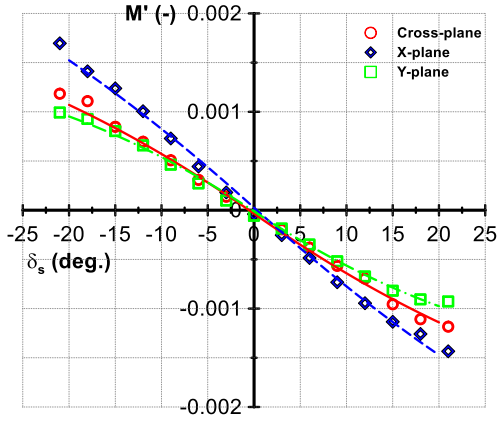

(**c**) Stabilizer moment about y-axis

Figure 8. Hydrodynamic force and moment of the stabilizers in vertical plane.

Table 1. This is a table. Tables should be placed in the main text near to the first time they are cited.

Title 1	Cross-rudder plane	X-rudder plane	Y-rudder plane
$X'_{\delta_r\delta_r}$	-5.27E-3	-8.81E-3	-9.06E-3
$X'_{\delta_s\delta_s}$	-4.91E-3	-9.66E-3	-7.40E-3
Y'_{δ_r}	8.62E-3	1.17E-2	8.07E-3
$Y'_{\delta_r\|\delta_r\|}$	-2.57E-3	-2.74E-3	-1.60E-4
Z'_{δ_s}	9.48E-3	1.12E-2	7.95E-3
$Z'_{\delta_s\|\delta_s\|}$	-6.97E-3	-4.28E-3	-4.47E-3
K'_{δ_r}	-4.48E-5	-7.61E-6	-8.11E-5
$K'_{\delta_r\|\delta_r\|}$	-1.43E-4	-2.38E-5	-2.11E-5
M'_{δ_s}	3.76E-3	4.84E-3	3.54E-3
$M'_{\delta_s\|\delta_s\|}$	-1.54E-3	-1.35E-3	-2.11E-3
N'_{δ_r}	-3.73E-3	-5.05E-3	-3.52E-3
$N'_{\delta_r\|\delta_r\|}$	9.67E-4	1.03E-3	-1.71E-4

A local view of pressure distribution on the rudder plane configurations are shown in Figures 9–11 for the static rudder test and static stabilizer test at deflection angle of 15 degrees. It is observed that the static pressure distributions are asymmetrical on the deflected blades of deflection of the Cross-rudder plane configuration. A stagnation region can be seen surrounding the leading edge of the left blades of the rudder plane configuration. Howerver, the asymmetrical pressure field on all

 doi:10.20944/preprints202404.0444.v1

blades in X-rudder plane and two inclined blade in Y-rudder plane configurations for any deflection angle are shown.

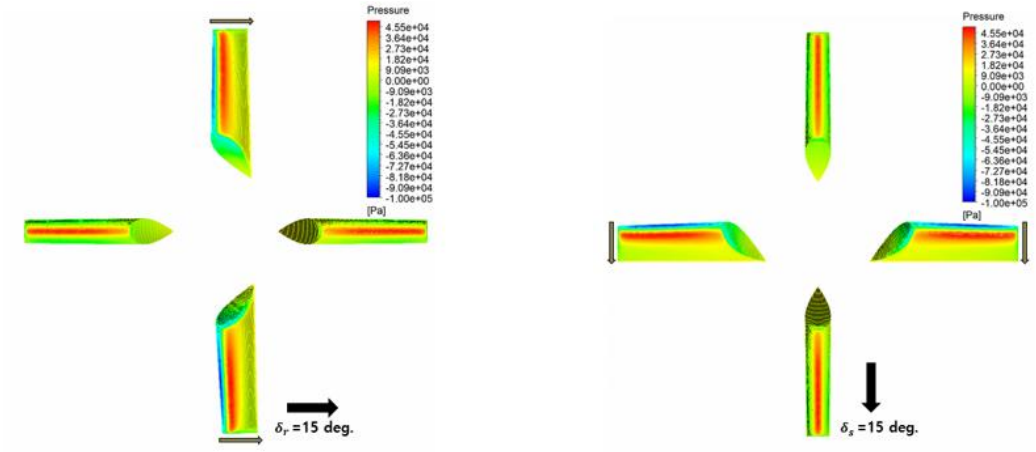

(**a**) (**b**)

Figure 9. Static pressure contour on the Cross-plane rudder configuration at angle of deflection of 15 degreea: (**a**) Deflection of rudders; (**b**) Deflection of stabilizers.

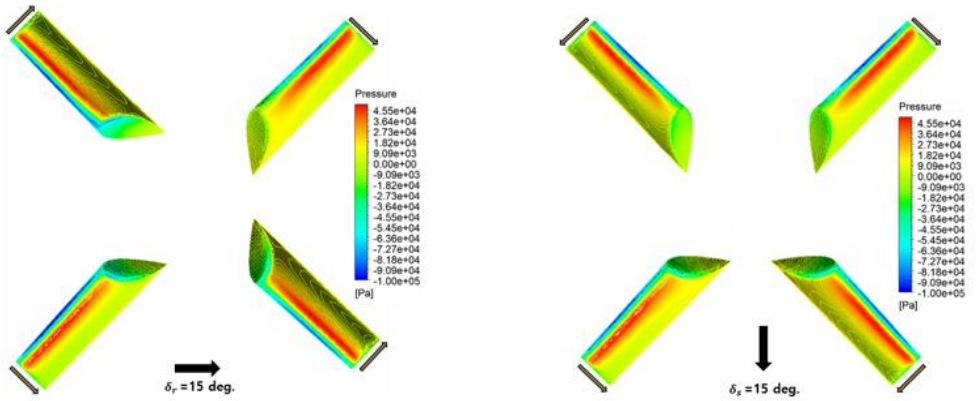

(**a**) (**b**)

Figure 10. Static pressure contour on the X- rudder plane configuration at angle of deflection of 15 degrees: (**a**) Deflection of rudders; (**b**) Deflection of stabilizers.

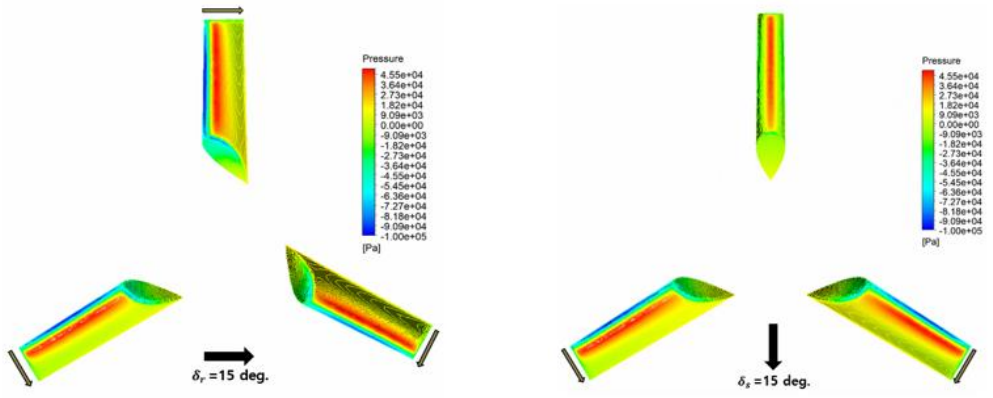

(**a**) (**b**)

Figure 11. Static pressure contour on the Y-rudder plane configurations at angle of deflection of 15 degrees (**a**) Deflection of rudders; (**b**) Deflection of stabilizers.

 doi:10.20944/preprints202404.0444.v1

5. Conclusions

The hydrodynamic force and moment of the three stern-plane configurations with the same span have been evaluated through simulation of fluid flow over the control surfaces with different angles of deflection using RANS method in Ansys Fluent code. The control surfaces are located at the stern of the hull of a submarine. The hydrodynamic force and moment acting on the Cross-rudder plane, X-rudder plane, and Y-rudder plane configurations have been obtained for estimating the hydrodynamic coefficients of the rudders and stabilizers. The hydrodynamic forces of the X-plane are largest in both the static rudder and static stern stabilizer test except for the roll moment that is the smallest value in comparison with the left rudders. The hydrodynamic force and moment of the rudder in the Cross-plane are smaller than those in the Y-rudder plane configuration. But hydrodynamic force and moment of stabilizers in Cross-rudder plane are larger than in the case of Y-rudder plane configuration. The first order derivative of Y-force of the X-rudder plane configuration is about 1.97 times and 1.31 times greater than the first derivative of Y-force of the Cross-rudder plane and Y-rudder plane configurations. The first order derivative of Z-force of the X-rudder plane configuration is about 1.18 and 1.41 times greater than the first order derivatives of the Cross-rudder plane and Y-rudder plane, respectively. The first order coefficients of the roll moment of the X-rudder plane are small in comparison with the roll moment of the left rudder plane configurations.

Funding Statement: Fund funds this research for Science and Technology Development of the University of Danang under project num-ber B2020-DN02-85.

References

1. Nguyen, T.T.; Yoon, H.K.; Park, Y.; and Park, C.. "Estimation of hydrodynamic derivatives of full-scale submarine using RANS solver." *J. Ocean Eng. Technol.* ***2018***, *Volume 20*, 386-392.
2. Cho, Y.J.; Seok, W.; Cheon, H.H; Rhee, S.H. Maneuvering simulation of an X-plane submarine using computation fluid dynamics. *Int. J. Nav. Archit. Ocean Eng.* ***2020***, *Volume 12*, 843-855.
3. Wu, S.J.; Lin, C.C.; Liu, T.L.; Su, I.H. Robust design on the arrangement of a sail and control planes for improvement of underwater vehicle's maneuverability. *Int. J. Nav. Archit. Ocean Eng.* ***2020***, *Volume 12*, 617-635.
4. Jeon, M.J.; Yoon, H.K.; Hwang, J.; Cho, H.J. Analysis of the dynamic characteristics for the change of design parameters of an underwater vehicle using sensitivity analysis. *Int. J. Nav. Archit. Ocean Eng.* ***2018***, *Volume 10*, 508-519.
5. Kim, H.; Ranmuthugala, D.; Leong, Z.Q.; Chin, C. Six-DOF simulation of an underwater vehicle undergoing straight line and steady turning manoeuvres. *Ocean Eng.* ***2018***, *Volume 150*, 102-112.
6. Zhang, Y.; Li, Y.; Sun, Y.; Zeng, J.; Wan, L. Design and simulation of X-rudder AUV's motion control. *Ocean Eng.* ***2017***, *Volume 137*, 204-214.
7. Zhang, Y; Li, Y; Zhang, G.; Zeng, J.; Wan, L. Design of X-rudder autonomous underwater vehicle's quadruple-rudder allocation with Le'vy flight character. *Int. J. Adv. Robot. Syst.* ***2017***, *Volume 14*, 1-15.
8. Broglia, R.; Cannarozzo, M.; Dubbioso, G.; Zaghi, S. Free Running Prediction of a Fully Appended Submarine: Effects of Stern Plane Configurations. In Proceedings of VI International Conference on Computational Methods in Marine Engineering, Rome, Italy, 15-17 June 2015.
9. Piaggio, B.; Vernengo, G.; Ferrando, M.; Mazzarello, G.; Viviani, M. Submarine Manoeuvrability Design: Traditional Cross-Plane vs. x-Plane Configurations in Intact and Degraded Conditions. *J. Mar. Sci. Eng.* ***2022***, *Volume 10*, 1-38.
10. Park, J.H.; Shin, M.S.; Jeon, Y.H. and Kim, Y.G. Simulation-Based Prediction of Steady Turning Ability of a Symmetrical Underwater Vehicle Considering Interactions Between Yaw Rate and Drift/Rudder Angle. *J. Ocean Eng. Technol.* **2021**, *Volume 35*, 99-112.
11. Ke, L; Ye, J.; and Liang, Q. Experimental Study on the Flow Field, Force, and Moment Measurements of Submarines with Different Stern Control Surfaces. *J. Mar. Sci. Eng.* ***2023***, *Volume 11*, 1-20.
12. Pan, Y.; Zhang, H.; Zhou, Q. Numerical simulation of unsteady propeller force for a submarine in straight ahead sailing and steady diving maneuver. *Int. J. Nav. Archit. Ocean Eng.* ***2019***, *Volume 11*, 899-913.
13. Han, K.; Cheng, X.; Liu, Z.; Huang, C.; Chang, H.; Yao, J.; and Tan, K. Six-DOF CFD Simulations of Underwater Vehicle Operating Underwater Turning Maneuvers. *J. Mar. Sci. Eng.* **2021**, *Volume 9*, 1-24.

 doi:10.20944/preprints202404.0444.v1

14. Guo, H.; Li, G.; Du, L. Investigation on the flow around a submarine under the rudder deflection condition by using URANS and DDES methods. *Appl. Ocean Res.* ***2023***, *Volume 131*, 1-28.
15. Vali, A.; Saranjam, B.; and Kamali, R. Experimental and Numerical Study of a Submarine and Propeller Behaviors in Submergence and Surface Conditions. *J. Appl. Fluid Mech.* ***2018***, *Volume 11*, 1297-1308.
16. Fureby, C.; Anderson, B.; Clarke, D.; Erm, L.; Henbest, S.; Giacobello, M.; Jones, D.; Nguyen, M.; Johansson, M.; Jones, M.; Kumar, C.; Lee, S.K.; Manovski, P.; Norrison, D.; Petterson, K.; Seil, G.; Woodyatt, B.; Zhu, S. Experimental and numerical study of a generic conventional submarine at 10° yaw. *Ocean Eng.* ***2016***, *Volume 116*, 1-20.
17. Fossen, T.I. In *Guidance and Control of Ocean Vehicles*. 3rd ed.; John Wiley and Son: Baffins Lane, Chichest West Sussex, England, 1999; pp. 168-180.
18. Menter, F. Two-Equation Eddy-Viscosity Turbulence Models for Engineering Applications. *AIAA* ***1994***, *Volume 32*, 1598-1605.
19. Wilcox C. D. *Turbulence Modeling for CFD*. 3rd Ed.; DCW Industries Inc.: 5354 Palm Drive, La Cafiada, California, America, 2006.
20. ITTC - Recommended Procedures and Guidelines: Practical guidelines for ship CFD application, 2011. https://ittc.info/media/1357/75-03-02-03.pdf.
21. Oh, K.J.; Kang, S.H. Full scale Reynold number effects for the viscous flow around the ship stern. *Computational Mechanics 1992*, Volume 9, 85-94.